Title

Chemical and Morphological Origins of Improved Ion Conductivity in Perfluoro Ionene Chain Extended Ionomers

Journal

Journal of the American Chemical Society, 141(34)

ISSN

0002-7863

Authors

Su, Gregory M

Cordova, Isvar A

Yandrasits, Michael A

et al.

Publication Date

2019-08-28

DOI

10.1021/jacs.9b05322

Peer reviewed

Chemical and Morphological Origins of Improved Ion Conductivity in Perfluoro Ionene Chain Extended Ionomers

Gregory M. Su,[†,§] Isvar A. Cordova,[†,§] Michael A. Yandrasits,[‡] Matthew Lindell,[‡] Jun Feng,[†] Cheng Wang,[*,†] and Ahmet Kusoglu[*,¶]

[†]*Advanced Light Source, Lawrence Berkeley National Laboratory, Berkeley, CA 94720, USA.*

[‡]*3M Corporation, St. Paul, MN 55144, USA.*

[¶]*Energy Conversion Group, Energy Technologies Area, Lawrence Berkeley National Laboratory, Berkeley, CA 94720, USA.*

[§]*These authors contributed equally to this work*

E-mail: cwang2@lbl.gov; akusoglu@lbl.gov

Abstract

The performance of ion-conducting polymer membranes is complicated by an intricate interplay between chemistry and morphology that is challenging to understand. Here, we report on perfuoro-ionene chain extended (PFICE) ionomers that contain either one or two bis(sulfonyl)imide groups on the side-chain in addition to a terminal sulfonic acid group. PFICE ionomers exhibit greater water uptake and conductivity compared to prototypical perfluorinated sulfonic acid ionomers. Advanced *in situ* synchrotron characterization reveals insights into the connections between molecular structure and morphology that dictate performance. Guided by first-principles

calculations, X-ray absorption spectroscopy at the sulfur K-edge can discern distinct protogenic groups and be sensitive to hydration level and configurations that dictate proton dissociation. *In situ* resonant X-ray scattering at the sulfur K-edge reveals that PFICE ionomers have a phase-separated morphology with enhanced short-range order that persists in both dry and hydrated states. The enhanced conductivity of PFICE ionomers is attributed to a unique multi-acid side-chain chemistry and structure that facilitates proton dissociation at low water content in combination with a well-ordered phase-separated morphology with nanoscale transport pathways. Overall, these results provide insights for the design of new ionomers with tunable phase-separation and improved transport properties and demonstrate the efficacy of X-rays with elemental sensitivity for unraveling structural features in chemically-heterogeneous functional materials for electrochemical energy applications.

1 Introduction

Research and progress on ion-conductive polymers (ionomers) are at the forefront for developing improved solid-electrolyte membranes for electrochemical energy conversion devices, such as polymer-electrolyte fuel cells, redox flow batteries, electrolyzers, and water-splitting devices.[1–8] A class of ionomers that has been widely used in electrochemical energy and water applications and consistently investigated is perfluorosulfonic acid (PFSA) ionomers, with Nafion being the most well-studied. Ionomers are attractive because of their highly selective ion conductivity combined with both chemical and mechanical stability. These advantageous properties are largely due to their unique chemically-heterogeneous morphology that results from phase separation between the stable semicrystalline backbone and hydrophilic side-chains.[1,9]

The phase-separated nano-domain network of ionomer membranes dictates transport properties and performance in energy-related applications. This nanoscale morphology is governed by hydration-driven phase-separation between hydrophilic ionic phases and hy-

drophobic backbone phases.[1,10] PFSAs consist of a polytetrafluoroethylene (PTFE) backbone and perfluorinated vinyl ether side-chains terminated with sulfonate groups (SO_3^-) and a counterion, typically a proton (H^+), forming sulfonic-acid groups (SO_3H). The chemical dissimilarity between the hydrophobic backbone and hydrophilic pendant side-chains leads to nanoscale (2-6 nm) phase separation.[1] The connectivity of the ion-containing, hydrophilic domains provides ion transport pathways while the PTFE backbone imparts chemical and mechanical stability. The degree of this phase-separation in response to hydration is primarily influenced by the ionomer chemistry, including the number of TFE repeat units in the backbone between side-chains, m_{TFE}, and the side-chain chemistry (Figure 1).[1,11–13] Side-chain chemistry and m_{TFE} collectively control a perfluorinated ionomer's equivalent weight (EW), the grams of dry polymer per mole of ionic group, which is inversely proportional to the ion-exchange capacity (IEC). The higher the EW, the lower the uptake and conductivity, all other factors being equal.[1,10] Thus, ionomer EW dictates hydration and transport properties, mechanical stability and ultimately its morphology and structure-function relationships.

Despite Nafion's long research history, perfluorinated ionomers with different side-chain chemistries and varying EWs have begun to attract interest. There is a need to develop alternative ionomers that can meet the ever-growing demand for diverse functionalities in many devices.[1,2,14–16] Development of next-generation membranes that have suitable conductivity under drier conditions requires fundamental understanding and control over their nano-morphology and ion-transport pathways. Conductivity in PFSAs increases with macroscopic swelling (e.g., humidification), which is driven by the molecular hydration in terms of water content per poly(anion) group and associated expansion of the mesoscale domain-network. However, the high humidity needed for enhanced conductivity requires efficient water management and creates challenges for ionomer performance under drier and hotter (dry-hot) conditions. Furthermore, high degrees of hydration can lead to excessive swelling, which may cause stability issues.[1,11] While increasing TFE repeat units enhances the ionomer

chain's ability to form more crystalline domains and improves stability, it also reduces the number of sulfonic acid groups per unit volume, or the charge density (IEC), thereby deteriorating transport.[1,15] One route to circumvent this dichotomy in ionomers is to alter the side-chain chemistry, potentially expanding the feasibility limits of high-IEC PFSAs.[11]

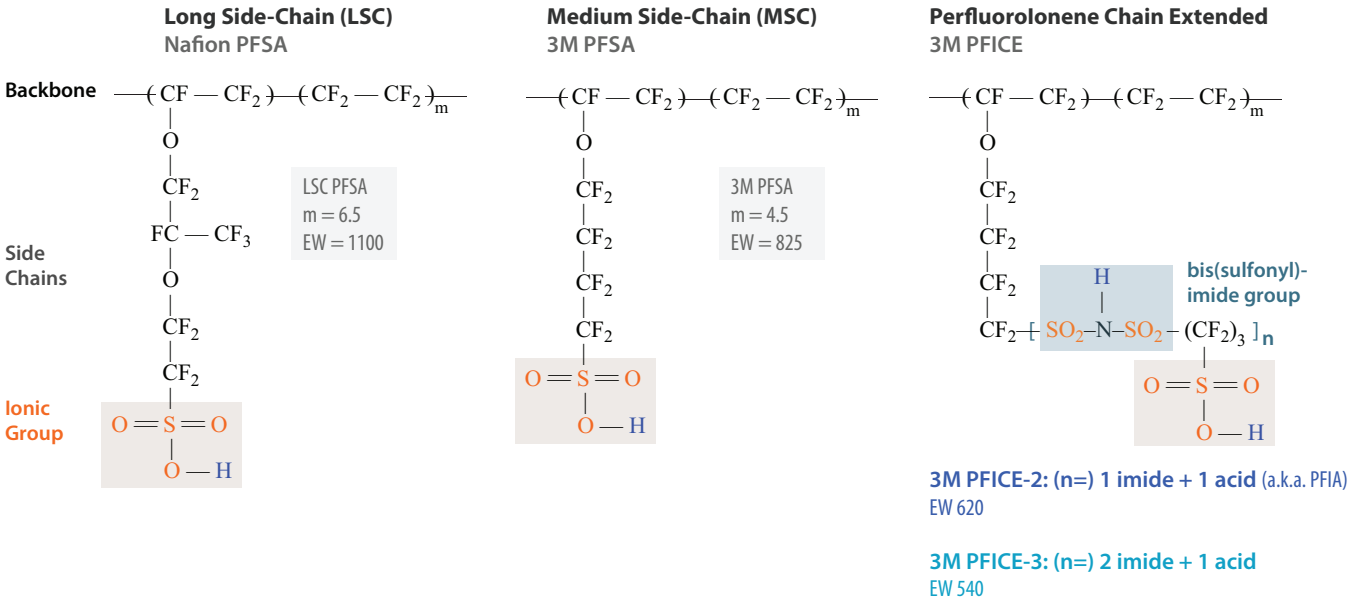

Figure 1: Chemical structures of the PFSA and PFICE ionomers studied in this work where n = 0 for PFSA and n = 1 or n = 2, for the PFICE-2 and PFICE-3, respectively. 3M PFSA ionomers share the same fluorocarbon backbone with a repeat unit of m = 4.5 (±0.5). In the main text, m is referred to as m_{TFE} to clarify it refers to the number of TFE repeat units in the backbone.

To meet these design goals, ionomers with modified chemistries have been developed to enhance conductivity at lower humidity levels.[13,15] 3M and Solvay have developed PFSA ionomers with shorter side-chains relative to Nafion, resulting in lower EW. However, very low equivalent weights can inhibit crystallization of the backbone and lead to excessive swelling and reduced stability in liquid water.[1,15] 3M has synthesized a series of alternative multi-acid side-chain (MASC) ionomers based on the medium side-chain 3M PFSA, where the number of protogenic groups on the side-chain is increased for the same backbone length (m_{TFE}). A promising chemistry belonging to this class is Perfluoro Ionene Chain Extended (PFICE) ionomers,[11,13,15] where the number of protogenic bis(sulfonyl)imide groups on the

side-chain can be controlled between n = 1 and 3 (Figure 1). One particular chemistry (n = 1, PFICE-2) is perfluoro imide acids (PFIA), which shares the same fluorocarbon backbone as the PFSA, but contains an additional imide acid group providing the secondary protogenic group (Figure 1). This approach has the advantage that for the same m_{TFE} needed for structural integrity along the backbone, two acid groups can be introduced, allowing a lower EW polymer with similar TFE content as the equivalent PFSA without any imide acid groups. In this case, starting with the same sulfonyl fluoride polymer, the PFSA generated would have an EW of 825 g/mol, but the PFIA would have an EW of 620 g/mol. This novel ionomer is being developed by 3M because of its notably higher proton conductivity at lower relative humidity (RH) than the parent PFSA, which results in improved performance in fuel cells under dry-hot conditions,[12,17–23] albeit with possible stability issues as its side-chain is prone to chemical degradation.[15,20,24] Despite recent studies on PFIA (PFICE-2), how this new bis(sulfonyl)imide group changes the hydration and structure-transport interplay in PFICE ionomers compared to PFSAs remains an open question. The disordered nano-morphology of PFSA ionomers, which is characterized by a broad ionomer peak in small-angle X-ray scattering (SAXS) experiments, makes it challenging to accurately establish hydration-dependent structure-transport relationships.[1] The chemically-heterogeneous nature of PFSA and PFICE ionomers presents unique challenges to elucidate the underlying origins of structure, creating a need for combinatorial characterization methods capable of resolving the differences among these chemistries while determining their role in ionomer structure-property relationships.

Energy-tunable X-rays can reveal element-specific bonding environments and spatial distributions at nanometer length scales in polymeric materials. This combined chemical and morphological information can uniquely complement hard X-ray scattering and other techniques to help unravel fundamental structure-property relationships. X-rays in the soft (∼150-2000 eV) and tender (∼2000-7000 eV) regimes are especially well suited for polymer materials because they span the core-level absorption energies of the common elements found

in polymers, for example, C, N, O, F, and S. Near edge X-ray absorption fine structure (NEXAFS) spectroscopy is sensitive not only to specific elements, but also local bonding environment and hence the presence of distinct functional groups.[25,26] Energy-dependent resonant X-ray scattering (RXS) leverages changes in the complex index of refraction, *n(E)*, near an absorption edge to enhance scattering contrast in materials with little electron density variation and reveal characteristic length-scales. Resonant soft X-ray scattering (RSoXS) has recently seen widespread use in many carbon-based materials such as carbon nanotubes,[27] liquid crystals,[28–30] proteins,[31,32] and polymers.[33–38] To date, RXS has not been applied to PFSA ionomers. Here, we showcase RXS at energies near the sulfur K-edge, around 2470 eV, which is ideal for studying proton-conducting ionomers for several reasons. Firstly, this energy range allows sensitivity and enhanced contrast specific to the important sulfur-containing protogenic groups in these materials. Furthermore, domain spacings on the order of a nanometer can be probed at this wavelength, an appropriate length-scale for the phase-separated morphologies these materials attain. X-rays near the sulfur K-edge can penetrate membranes that are 10s of micrometers thick, relevant to the thicknesses used in energy conversion devices such as fuel cells. Sulfur K-edge RXS has seen minimal use in polymer systems,[39] largely due to the limited number of beamlines capable of doing scattering experiments in this energy range.

Herein, we show that PFICE ionomers exhibit higher conductivity compared to PFSAs across a range of relative humidity values (20%-80%), even at the same degree of molecular hydration. X-ray scattering and absorption spectroscopy coupled with *ab initio* calculations reveal that the unique chemistry of the PFICE ionomers results in a phase-separated morphology with larger correlation lengths and greater short-range order and favorable hydrogen bonding configurations of water molecules, revealing a trend dependent on the number of bis(sulfonyl)imide groups (n). Moreover, NEXAFS spectroscopy combined with energy-dependent scattering profiles suggest that PFICE ionomers have a more spatially homogeneous distribution of hydrated phases, especially under dry (ambient) conditions. The

findings in this paper not only provide insight into the critical role of side-chain chemistry in structure-property relationships of ionomers and the molecular parameters to improve transport, but also demonstrate the potential of tender X-rays with elemental sensitivity for characterization of similar ion-containing polymers.

2 Methods

2.1 Materials

3M Ionomers with multiple bis(sulfonyl)imide groups per side chain, designated herein as perfluoro ionene chain extended (PFICE), were synthesized by a sequential reaction process in 3M Corporate Research Materials Laboratory (St. Paul, MN). Syntheses of PFICE-2 and PFICE-3 were accomplished by post-polymerization modification of the sulfonyl fluoride form precursor to 3M 825 PFSA, and more details are provided in the Supporting Information.

The dispersions of synthesized ionomers were coated in protonated H^+ form using a Gardco notch bar onto 2 mil Kapton or PTFE sheets supported on and taped to 1/8-inch-thick glass plates, loosely covered with an aluminum pan, and dried in a forced air oven upon ceramic supports at 120 °C for 30 minutes. The glass plate support was replaced with aluminum and films were further heated to 145 °C for 15 min, and then annealed at 200 °C for 10 min followed with a thermal quench to ambient conditions by pulling out of the oven to cool. Film thicknesses were characterized by drop gauge micrometers with 1 μm resolution. (See Table 1). Equivalent weights of membranes were determined after drying approximately 0.5 g film sections at 120 °C for 20 minutes, weighing the dry sample, and placing it into 50 g of 1 M NaCl(aq). The membranes were allowed to ion exchange for more than 4 hours with gentle agitation by rolling or shaking in a bottle. The HCl generated was titrated with 0.03 M NaOH to determine the ion exchange capacity of the film. All the samples were peeled off of the Kapton or PTFE films and tested as-received. In some experiments, a Nafion 211 PFSA membrane purchased from Ion Power Inc. (New Castle,

DE) was used for comparison. The chemical structures and properties of the polymers are summarized in Figure 1 and Table 1, respectively.

Table 1: Ionomer membranes investigated in this study

Chemistry	# imide groups	EW [g/mol]	Thickness [μm]
Nafion (211)	0	1100	25
PFSA (3M)	0	825	20-21
PFICE-2	1	620	22-23
PFICE-3	2	540	24-27

2.2 X-ray absorption spectroscopy and X-ray scattering

NEXAFS experiments were conducted at the Advanced Light Source (ALS) bending magnet beamline 5.3.1. NEXAFS data was collected in fluorescence yield (FY) mode using a Vortex-EX detector at an angle of 45° from the incident beam or in transmission mode using a photodiode. Soft X-ray NEXAFS at the oxygen K-edge was collected under high vacuum at ALS beamline 11.0.1.2[40] in FY mode, where a CCD detector was used to detect the fluorescent photons. For normalization, a line was regressed to the pre-edge region and a polynomial regressed to the post-edge region using the Athena software package.[41]

Resonant X-ray scattering measurements were done in a transmission geometry with a sample-detector distance of about 345 mm, and 2D scattering patterns collected on a Pilatus 300K detector. 2D scattering images were azimuthally averaged to generate 1D intensity vs. q scattering profiles. These profiles were fit with two Voigt function lineshapes, one at lower q (around 0.05 Å^{-1}) for the intercrystalline peak, and one at higher q (around 0.15 Å^{-1}) for the ionomer peak. A representative example is shown in the Supporting Information. In addition, the intensity of the scattering invariant[42,43] for each energy was approximated by plotting the Iq^2 profiles for each energy, where a Gaussian fit was used to extract each ionomer peak's FWHM and area.

For experiments on dry samples, PFSA membranes were attached to a metal plate with an opening for X-ray transmission. The 20 μm thick membranes are very robust and did

not need additional support. Samples were placed in an enclosed chamber with continuous flow of helium to reduce air scattering.

For measurements of wet samples, membranes were soaked in deionized water for at least 4 hours then cut into small (roughly 1.5 mm^2) pieces so that they could be loaded into a vacuum-compatible flow cell (Protochips) designed for *in situ* measurements with soft X-rays in a transmission configuration. This cell encapsulated the pieces of membrane between two water-tight 50 nm thick Si_3N_4 windows. Deionized water was flowed through the cell at a rate of 300 μL/hr with a programmable Harvard Apparatus Pump 11 Elite syringe pump.

Hard X-ray small-angle X-ray scattering (SAXS) experiments were performed at beamline 7.3.3 of the Advanced Light Source (ALS). The X-ray wavelength used was $\lambda = 0.124$ nm, with a monochromator energy resolution of E/dE of 100, and the presented patterns were collected using a 2D Dectris Pilatus 2M detector (172 μm x 172 μm pixel size). SAXS experiments of the hydrated ionomers were conducted *in situ* by immersing the samples in custom-designed solution cells enclosed with X-ray transparent Kapton^{TM} windows, as described previously.[10,44] For liquid-water experiments, the samples were equilibrated for at least 12 hours and then transferred to the cells, which were filled with DI water. All of the experiments were carried out at 25 °C. The collected two-dimensional scattering patterns were azimuthally integrated to generate 1-D intensity profiles, I(q), which were corrected for background scattering. From the SAXS data, hydrophilic-domain spacing and the full width at half maximum (FWHM) were calculated using a Gaussian fit to the (ionomer) scattering peaks. Experimental details are provided elsewhere.[10,44]

2.3 Computational methods

Since sulfur atoms are only on the side-chains of PFSAs, each material system was modeled as a single SO_3H-terminated side-chain attached to fragment of the PTFE backbone consisting of four -CF_2- units. The geometry of these structures was optimized using density functional theory (DFT) at the B3LYP level of theory with a 6-31G(d,p) basis set.

X-ray absorption spectra were simulated based on the DFT-optimized structures using the Plane-Wave Self-Consistent Field (PWSCF) code within the Quantum-ESPRESSO package. The Perdew-Burke-Ernzerhof (PBE) form[45] of the generalized-gradient approximation (GGA) to the exchange-correlation energy in DFT was used with ultrasoft pseudopotentials.[46] Transition amplitudes were calculated based on Fermi's golden rule.[25] Initial states are the 1s orbitals of the S atoms and final states are the unoccupied Kohn-Sham eigenstates determined from a self-consistent field calculated within the eXcited electron and Core Hole (XCH) approach,[47] which is based on constrained-occupancy DFT.[48,49] Simulated S K-edge profiles were shifted by a value of 2467.2 eV to align the calculated spectra to a physically meaningful energy range. The computed transitions were numerically convoluted with a 0.2 eV Gaussian line shape to create a continuous spectrum. Local or semi-local functionals, including the PBE-GGA functional used here, are known to underestimate band gaps and/or band widths.[50,51] This can result in spectra that are compressed along the energy axis. Hybrid exact exchange functionals[52] or first-order perturbation theory, like in the GW approximation,[53,54] can address this discrepancy to some extent. For the method used here, where a self-consistent representation of the core-excited state is needed, going beyond perturbation theory would be required. Furthermore, hybrid functionals are very computationally expensive. Therefore, rigorous efforts to address the overestimation of band gaps and band widths were not suitable for this study. However, to qualitatively improve agreement of peak separations between simulations and experiments, a dilation factor of 1.2 was applied to all S K-edge simulations. Although this is a somewhat arbitrary value, similar dilation factors have been used for K-edge XAS simulations,[55] and further studies would be required to more precisely determine the best dilation factor for sulfur K-edge predictions. The interpretation of the simulated XAS spectra would remain the same regardless of the use of a dilation factor.

2.4 Membrane water uptake

Membrane water uptake as a function of relative humidity (RH) was measured with a dynamic vapor-sorption (DVS) analyzer (Surface Measurement Systems, UK) at 25 °C.[44,56] First, the samples were dried in the DVS at 0% RH and 25 °C for 2 hours to set a standard dry state with initial sample weight, M_0. The samples were then humidified from 0% to 90% RH with an increasing RH interval of 10%, and then to 98% RH, using pre-humidified nitrogen feed. Samples were dehumidified/dehydrated back to 0% RH following the same RH values and interval, but in the opposite sequence. Water uptake of the membrane ΔM_W was continuously determined from the weight change with respect to the initial ("dry") weight, M_0. At each RH step, the samples were equilibrated for a minimum of 2 hours or until the change in the sample weight, $\Delta M_W/M_0$, was less than 0.005%/min. Due to the distinct nature of side-chains with additional protogenic groups, the commonly used measure of local hydration, i.e., water content, λ, is described as the number of water molecules per protogenic group (instead of sulfonic acid group, SO_3^-) and calculated from the measured water uptake, $\Delta M_W/M_0$ as:

$$\lambda = \frac{mol\ H_2O}{mol\ (R - H^+)} = \frac{\Delta M_W/18}{M_0/EW},$$

where EW is the equivalent weight of the membrane in g/mol and the molecular weight of the water is 18 g/mol. Equivalent weight and IEC are used interchangeably in this study, as they are inverses of each other via the relationship: $EW = 1000/IEC$. Lastly, the residual water in the membrane that is present at 0% RH at 25 °C, λ_{res}, was also measured from the weight change after heating the samples at 120 °C for 30 minutes.

2.5 Membrane conductivity

In this study, the proton conductivity of the membranes was measured as a function of RH at controlled temperature using a Membrane Test System (MTS) (MTS740) equipped with

a four-electrode BT-110 conductivity clamp (Scribner Associates, Inc.). Membranes were cut into rectangular specimens with a dimension of 10 mm x 35 mm and placed onto the clamp. Samples were first kept at 70% RH and 30 °C under nitrogen atmosphere for 2 hours. Afterward, the samples were dehumidified to 20% RH with intervals of 10% RH, and then hydrated to 90% with an increment interval of 10% RH, then to 98% RH, using a protocol similar to that used for the water-uptake measurements as described above. Samples were preconditioned for at least 30 min at each step and then the membrane resistance was measured using a Solartron 1286 DC potentiostat. The in-plane conductivity was calculated from $\kappa = L_{IP}R/A$, where L_{IP} is the distance between inner voltage electrodes (0.425 cm), R is the measured resistance of the membrane (Ω), and A is the cross-section area. Change in membrane thickness with humidity was estimated from hydration data to account for dimensional changes. Details of the procedure were previously reported for PFSAs and other ionomers.[44,57,58]

3 Results and discussion

3.1 PFICE ionomers exhibit enhanced water sorption and conductivity

Hydration behavior of PFICE and PFSA membranes are displayed in Figure 2. Overall, imide-containing ionomers absorb more water than PFSA based on macroscopic mass uptake (Figure 2). In fact, both PFICE-2 and PFICE-3 have similar mass uptake across the entire RH range. When sorption is quantified in terms of local hydration using water content per protogenic group, λ, the trends remain the same, even though the difference between PFSA and PFICE is reduced. This is because the latter has a lower EW (more protogenic groups), therefore for the same macroscopic mass uptake, water is distributed among a higher number of ionic groups, which reduces the average amount of water molecules attached to each protogenic group. A noteworthy observation is the water uptake at lower RHs, especially

the residual water at 0% RH, which is significantly higher for PFICE membranes compared to PFSA. Thus, the impact of the imide groups on membrane water uptake manifests itself stronger in dry conditions where PFICE membranes have better water retention capacity. Generally, this illustrates how various factors including the number of protogenic groups and side-chain length, need to be optimized.

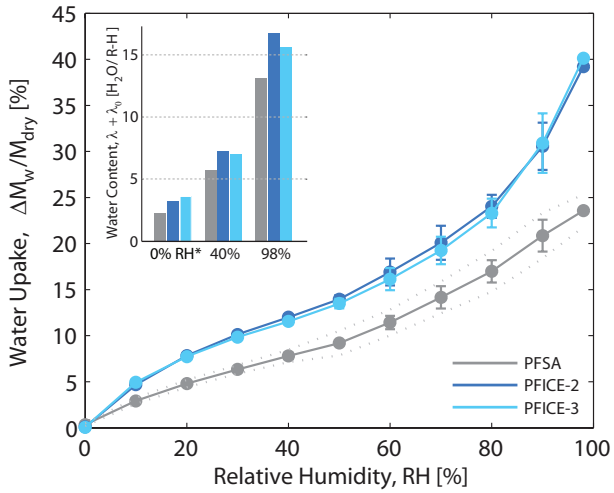

Figure 2: Sorption behavior of the PFSA and PFICE ionomers as a function of relative humidity (RH) is shown in terms of mass uptake at 25 °C. The inset shows water content per protogenic group, λ, at 25 °C for select RH values, including the residual water. Values at 0% RH represent the residual water content present in the ionomer at room temperature, and were measured by drying the samples at elevated temperature.

PFICE ionomers exhibit higher conductivity than PFSA, not only at the same RH, but also at the same λ, as shown in Figure 3. The latter is particularly critical as it signifies the key role of local hydrated structure in transport. These results collectively pinpoint to an enhanced transport functionality for the same backbone, likely due to changes in local environment around the imide-containing side-chain and ordering of the ionic-domain network.

Insight into the distinct chemical nature and phase-separated morphology of PFICE ionomers in device-relevant geometries is needed to understand the basis of its improved water uptake and conductivity relative to PFSA. This will not only shed light onto the unique features of PFICE ionomers, but also help build a fundamental molecular-level understanding

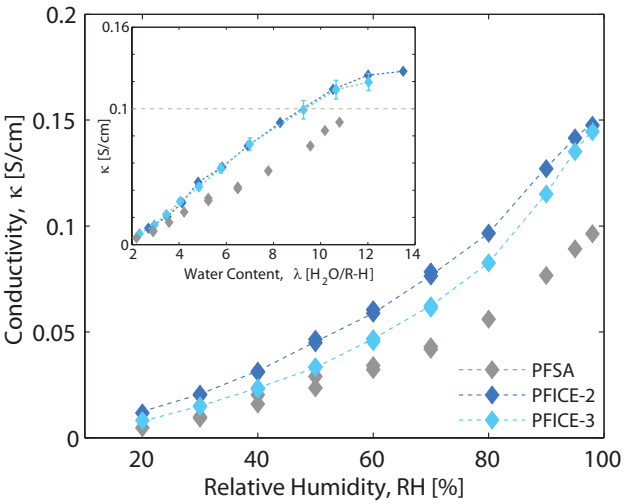

Figure 3: Proton conductivity of the PFSA and PFICE membranes measured at 30 °C plotted as a function of RH. The inset depicts the conductivity corrected for RH-dependent thickness change as a function of water content per protogenic group, λ.

of structure-function relationships to design next-generation ionomer materials.

3.2 NEXAFS spectroscopy is sensitive to the local sulfur environment

NEXAFS spectroscopy probes transitions of core-level electrons to unoccupied states.[25] Previous work has utilized NEXAFS spectroscopy to probe chemical bonding of Nafion PFSAs in the soft X-ray regime[59] and near the sulfur K-edge.[60,61] Since the sulfur K-edge spectrum is sensitive to chemical environment around the sulfur atoms, it can distinguish between sulfur atoms in the sulfonic acid functional group and sulfur atoms in the bis(sulfonyl)imide groups. Scattering contrast can also vary greatly at energies near an absorption edge.[34,62] Therefore, it is important to know the absorption profiles of the ionomers in order to determine which energies will optimize scattering intensity in RXS experiments.

The sulfur K-edge NEXAFS spectra of the four ionomers studied here depict an absorption spectra similar to those previously reported for PFSAs, with notable differences for PFICE-2 and PFICE-3 due to their distinct side-chain chemistry, as shown in Figure

4. Nafion and the 3M PFSA have only one unique sulfur atom in the sulfonic acid group. PFICE ionomers have both sulfonic acid groups and bis(sulfonyl)imide groups that have sulfur atoms in a different bonding environment. Thus, PFICE ionomers provide a unique material system that demonstrates the potential of sulfur K-edge NEXAFS to delineate the local chemical environment of distinct sulfur atoms. The simulated spectra of PFICE-2 depicted in Figure 4a clearly shows that the lowest energy transition (shoulder-like feature at 2477.6 eV) originates from the bis(sulfonyl)imide group (colored in red), explaining the lower energy absorption edge onset for PFICE-2 and PFICE-3 compared to Nafion and the 3M PFSA observed experimentally. This can be expected considering the nitrogen atom bonded to the sulfur in the bis(sulfonyl)imide group is less electronegative compared to oxygen. This lowest-energy transition in PFICE ionomers is σ^*_{S-N} in character, as shown by the density distribution of the core-excited state in Figure 4b. The main peak at around 2480 eV arising from the sulfonic acid group has been attributed to a σ^*_{S-C} transition,[60,63] and the first core-excited state for that sulfur atom illustrates this, also shown in Figure 4b.

NEXAFS spectroscopy has the potential to go beyond local bonding environment and probe the degree of hydration and hydrogen bonding configuration around sulfonic acid or bis(sulfonyl)imide groups. Hydration is a critical parameter that controls proton dissociation and resulting conductivity, and the ability to probe hydration state would provide unique fundamental insight into connections among chemistry, structure, and conductivity. First-principles simulations are necessary to understand details of NEXAFS spectra that cannot easily be determined from experimental data alone.[47,64–66]

Previous work has looked at Nafion sulfur K-edge NEXAFS under wet and dry conditions and varying potential bias. It was shown that the intensity of the higher energy shoulder feature compared to the main peak increased in wet Nafion compared to dry Nafion, and this was attributed to a reduced ionization of the sulfonic acid in dry conditions and a greater population of the sulfonic acid moiety.[60] The energy separation between the main peak and the shoulder feature decreased under wet conditions. Furthermore, the chemistry

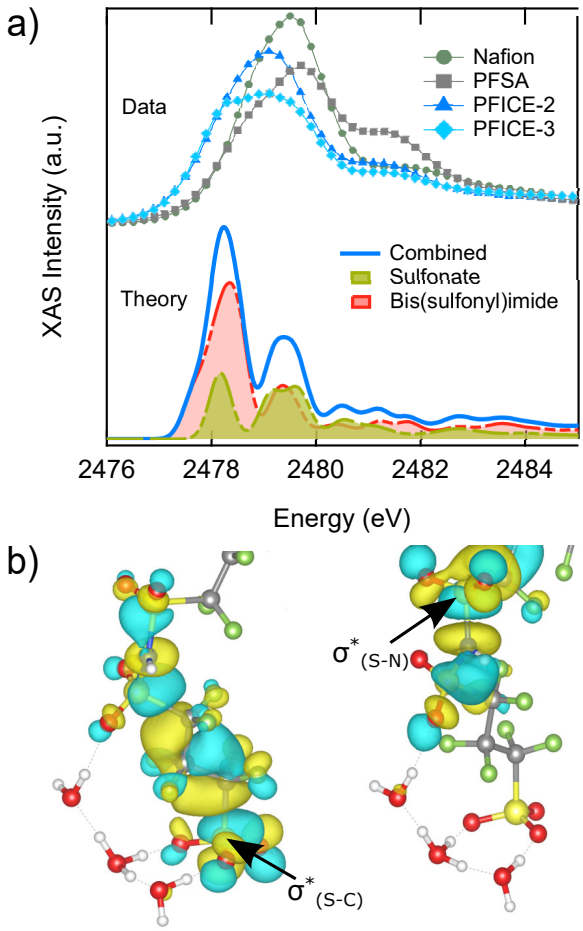

Figure 4: Sulfur K-edge NEXAFS spectra of the PFSA and PFICE ionomers reveal spectroscopic signatures of the two unique sulfur-containing protogenic groups. Experimental and simulated NEXAFS profiles are shown in (a). The simulated spectra is for a single side-chain unit of PFICE-2, and the contributions from the sulfonic acid and the bis(sulfonyl)imide groups are shown as shaded traces. Density distributions of the electronic component of the lowest-energy core-excited state for a sulfur atom in the sulfonic acid group (left) and the bis(sulfonyl)imide group (right) are shown in (b). The positive and negative phases of the wavefunction are shown as teal and yellow regions, respectively. The excited sulfur atom is indicated with an arrow.

of the functional group bound to the sulfonic acid was found to have a noticeable effect on the shoulder-like feature at higher energy (around 2481 eV).[60] Here, the relative intensity of the shoulder feature is markedly higher in the 3M PFSA compared to Nafion (Figure 4a), suggesting that NEXAFS has captured a significant difference in the molecular structure of these two sulfonic acid environments. The -$CF_2CF_2CF_2CF_2$- group bound to the sulfonic acid in the 3M PFSA may be overall more electronegative than the -OCF_2CF_2- group in

Nafion, reducing electron density of the p-electrons on the carbon atoms and increasing the intensity of the shoulder feature. The multiple distinct sulfur atoms per side-chain in the PFICE ionomers makes deciphering the NEXAFS spectra more challenging, underscoring the need for complementary first-principles calculations. Despite the lack of energy resolution in the experimental data to see individual transitions, simulations suggest that PFICE-3 has a higher relative intensity of the low-energy shoulder (near 2478 eV) compared to the main absorption feature (2479 eV) due to the greater amount of bis(sulfonyl)imide groups per side-chain in PFICE-3, which contributes to the lowest-lying transitions.

DFT-computed spectra of a PFICE-2 side-chain reveals the dependence of the sulfur K-edge NEXAFS spectra on the number of water molecules hydrogen-bonded around the sulfur-containing functional groups, as shown in Figure 5. The geometry-optimized molecular structures in the insets of Figure 5 show that three water molecules are needed to dissociate the proton of the sulfonic acid group, and a similar trend is seen for proton dissociation at the bis(sulfonyl)imide group, in agreement with previous computational studies.[67,68] The core-level transitions shift in energy with hydration. The first excited state transition shifts to higher energy when water molecules are present, and this is noticeable even with one added water molecule. This trend continues when considering the absorption spectra of the sulfur atoms in the sulfonic acid group (Figure 5a) or the bis(sulfonyl)imide group (Figure 5b). The higher energy feature in the simulated spectra of an -SO_3H terminated side-chain (at 2480 eV) is pronounced and well separated from the lower energy peaks in the dry state (Figure 5a). However, addition of water molecules increases the number of transitions in that range, causing the higher energy peak to appear merged with the main absorption feature. This is generally similar to an earlier study, although it did not include distinct water molecules in the model for hydrated Nafion, but only compared a $CHF_2CF_2SO_3^-$ (wet) fragment to a $CHF_2CF_2SO_3H$ (dry) fragment.[60] Overall, simulations suggest the presence of just one water molecule can lead to a sufficient change in electron density to influence the NEXAFS profile. Plots of the electron density distribution of various final state orbitals for

different hydration states (zero, one and three added water molecules) around the sulfonic acid group are shown in the Supporting Information.

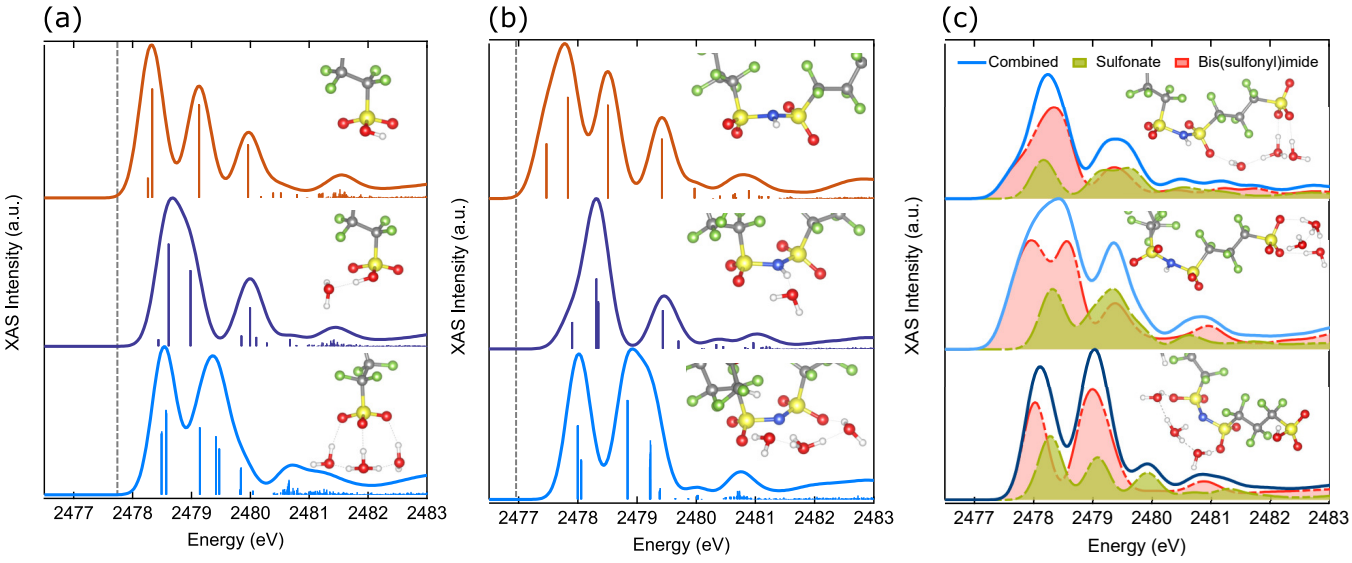

Figure 5: Simulated sulfur K-edge NEXAFS of the PFICE-2 ionomer with increasing degrees of hydration around specific protogenic groups and different hydration configurations. Spectroscopic changes at the sulfonic acid group due to increasing number of additional water molecules are shown in (a). The top panel is an -SO_3H terminated side-chain, the middle panel shows the spectrum for one additional hydrogen bonded water molecule, and the bottom panel three hydrogen bonded water molecules. The corresponding structures are shown in the insets. The vertical lines represent the individual core-level transitions, and the solid curves are the continuous, Gaussian-convoluted spectra. A similar series of simulated spectra with varying amounts of additional water molecules around the bis(sulfonyl)imide group is shown in (b). Note the individual transitions of only one sulfur atom in the bis(sulfonyl)imide group are shown. The dotted lines are guides to the eye to indicate the absorption onsets. The effect of different hydrogen-bonding configurations for three water molecules surrounding a PFICE-2 ionomer side-chain is shown in (c). The top panel in (c) shows the water molecules bridging the sulfonic acid and bis(sulfonyl)imide groups, the middle panel depicts all three water molecules surrounding the sulfonic acid group, and the lower panel all three water molecules around the bis(sulfonyl)imide group.

Proton dissociation is dependent on factors including the number and proximity of protogenic groups, side-chain conformations affecting the relative orientation among them, overall charge delocalization, and the hydrogen bonding structure of surrounding water molecules. For a given temperature and humidity, an ionomer's ion conductivity is affected by charge density and degree of hydration. Hydration capacity is also controlled by EW; the lower the EW (or m_{TFE}), the easier acid groups can accommodate additional water molecules due to

reduced resistance to swelling of hydrophilic domains by the backbone chains. Proton transport is influenced by the proximity between adjacent side-chains (m_{TFE}), and there is an interplay among backbone conformation, water content and coordination near the protogenic groups.[69,70] The minimum number of water molecules required to initiate proton dissociation is influenced by the separation of the charges not only on a given side-chain, but also between adjacent side-chains, i.e. the backbone length: the shorter the backbone, the lower the hydration required to transfer protons to the hydration shell of water.[69–71] Molecular simulation studies have shown that the number of water molecules needed for spontaneous dissociation is typically consistent with the strength of the acid, that is, the stronger the acid, the fewer the water molecules needed for proton dissociation.[72] The bis(sulfonyl)imide group has a greater gas phase acidity compared to sulfonic acid.[73] This would imply that proton dissociation occurs first at the bis(sulfonyl)imide site. However, *in situ* infrared spectroscopy studies suggest that it is the sulfonic acid group in PFICE-2 that ionizes first with increasing hydration levels.[17] This finding has been attributed to the hydrogen bonding structure of water molecules at minimal hydration conditions. Computational studies have shown that the first proton to dissociate in PFICE-2 occurs at a hydration level of three water molecules. The lowest energy structure is attained when the three water molecules bridge the sulfonic acid and bis(sulfonyl)imide groups, and this results in the sulfonic acid proton dissociating first.[68] DFT-optimized geometries in this work show a consistent trend (Figure 5c), and furthermore reveal that both protons on the side-chain of PFICE-2 can dissociate when six added water molecules are present (shown in the Supporting Information). A similar first proton dissociation trend is expected for PFICE-3, and this is evidenced by the low hydration structures of PFICE-3 shown in the Supporting Information. Interestingly, seven water molecules may be required to dissociate a second proton from one of the bis(sulfonyl)imide groups in PFICE-3, as seen from the the hydrated geometries (Supporting Information). The second proton to dissociate could be at the bis(sulfonyl)imide group farthest away from the sulfonate group, and this is possible due to the greater configurational freedom of the longer

side-chain on PFICE-3 and the relative orientations of the oxygen atoms and acidic protons on the two bis(sulfonyl)imide moieties with respect to the sulfonic acid group. Such findings illustrate the important interplay among the distance between protogenic groups, configurational freedom, hydration level, and hydrogen bonding and shed light onto the enhanced proton transport properties of PFICE ionomers.

The ability to distinguish among different hydration configurations for a given hydration level (λ) would allow unique insight into the intermolecular interactions controlling proton dissociation and conductivity. Simulations reveal that NEXAFS spectroscopy can be sensitive to hydration configuration for a given number of added water molecules, as shown in Figure 5c for PFICE-2 with three added water molecules. One noticeable distinction is a shift to higher energy of the lowest-lying transition, which originates from the bis(sulfonly)imide group, when all three water molecules surround the bis(sulfonyl)imide group. Since the configuration with water molecules bridging the two protogenic groups has been shown to be favorable,[68] the higher energy absorption onset should only be evident above minimum hydration conditions. Initial NEXAFS data of wet PFSA and PFICE ionomers is shown in the Supporting Information and compared to dry spectra. Overall, Nafion and the PFSA ionomer exhibit a more noticeable change in the NEXAFS profiles between wet and dry conditions compared to the PFICE ionomers. This supports the idea that PFICE has a greater amount of water molecules in a low-RH environment, as shown in the water uptake data in Figure 2. In general, the shoulder feature at around 2481 eV becomes less pronounced in wet ionomers, and this is in overall agreement with simulated spectra. A shift in the absorption onset upon hydration is not obvious in the experimental data. Although this is predicted by simulations, the calculated spectra reveal that only one additional water molecule is needed to shift the absorption onset to higher energy. In the actual membrane, some water molecules remain hydrogen bonded to the ionic groups even under dry conditions, so this effect would be difficult to discern. NEXAFS spectroscopy coupled with theory is useful in elucidating hydration effects, and this will be especially useful as improvements in beamline capabilities

allow for higher energy resolution near the sulfur K-edge.

NEXAFS collected at the oxygen K-edge sheds further insight on differences between PFICE and PFSA in terms of chemistry and water content induced by the bis(sulfonyl)imide groups. The strongest features observed are similar across all four ionomers, as shown in the Supporting Information, and consistent with previously reported spectra.[59] However, only PFICE-2 and PFICE-3 have a shoulder feature near 534 eV, a core-level absorption feature that has not been observed in PFSA materials. This is consistent with the simulated O K-edge results of PFICE-2 with six added water molecules (shown in the Supporting Information), suggesting that this shoulder feature originates from the bis(sulfonyl)imide groups. Furthermore, the surrounding water molecules exhibit a peak at 535 eV, so the shoulder feature for PFICE-2 and PFICE-3 also implies better water retention in these imide-containing ionomers.

3.3 Resonant X-ray scattering reveals stronger order in PFICE

Hydrophilic domain spacing, ordering, and connectivity are important parameters related to phase separation that determine transport pathways. These morphology features need to be understood to construct relationships between molecular structure and conductivity.[74] SAXS can reveal the degree of phase separation in ionomer membranes. Because ionomers, and many similar charge-containing polymers in general, are relatively disordered, the peaks in SAXS tend to be broad without higher-order peaks visible, indicating only short-range order in these materials. This can make it challenging to fit scattering data to specific models. Nevertheless, X-ray scattering is an indispensable tool to probe statistically significant morphology information in ionomer membranes.[1,9,75] Hard X-ray SAXS has elucidated morphology differences between the 3M PFSA of different EW's and Nafion. The phase-separation correlation length (d-spacing) of 3M PFSA ionomers linearly increases with water content (λ), but with a smaller slope compared to Nafion 1100 EW.[10] Further SAXS studies of the nanoswelling of the ionic domains of the 3M PFSA revealed a better connected morphol-

ogy.[76] Doping the 3M PFSA ionomer with 12-phosphotungstic acid (HPW) alters solvent interactions with the ionic group promoting interconnected proton conducting channels.[77] To date, energy-tunable RXS has not been reported for PFICE ionomers or perfluorinated ionomers in general. Here, we leverage RXS at energies near the sulfur K-edge to enhance scattering contrast of ionomer films. In addition to the aforementioned morphological details elucidated by SAXS, RXS reveals the key features of domain sizes and correlation lengths that can be related to local ionomer chemistry and degree of hydration, thus helping develop design principles for ion-conductive materials.

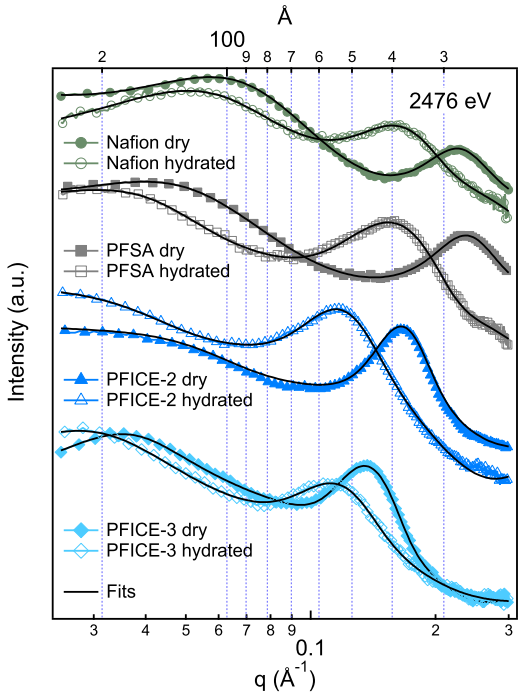

Figure 6: Transmission resonant X-ray scattering profiles at 2476 eV of dry (ambient) and hydrated (immersed in liquid water) ionomer membranes show changes in domain spacing as a function of side-chain chemistry and water content. Scattering of dry membranes is shown as lines with solid symbols, and scattering of membranes submerged in water is represented as lines with open symbols.

RXS clearly shows the phase-separated nano-structure of Nafion, PFSA, and PFICE ionomers (Figure 6). All of the ionomers exhibit a scattering peak between 0.1 $Å^{-1}$ and 0.25 $Å^{-1}$, corresponding to the average separation between hydrophilic domains, i.e. d-spacing, and another peak at lower q in the 0.03 $Å^{-1}$ to 0.07 $Å^{-1}$ range representative of the distance

between semi-crystalline domains. We focus primarily on the hydrophilic domain peak, or ionomer peak, located at higher q (smaller d-spacing), since these form the interconnected domain-network for transport of water and ions.

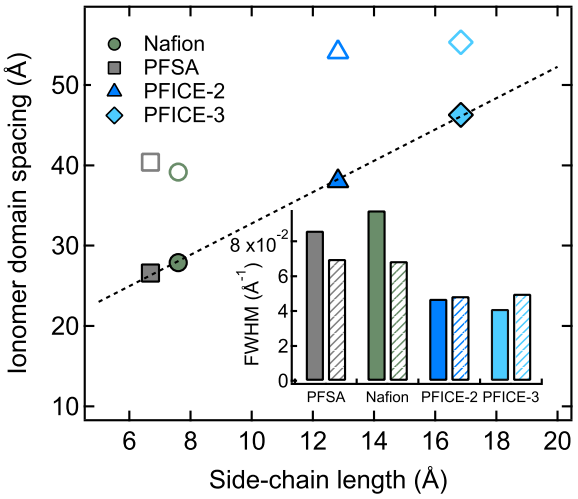

Figure 7: Hydrophilic ionomer domain spacing, determined from RXS, plotted as a function of side-chain length. Filled symbols are for samples under dry (ambient) conditions, and open symbols are hydrated samples immersed in liquid water. Side-chain length was determined as the distance between the sulfur atom in the sulfonic acid group and the carbon atom on the backbone that the side-chain is attached to based on the DFT-optimized geometry of a single monomer. Inset shows the full width at half maximum (FWHM) of ionomer peaks, where dry samples are represented as solid filled bars, and hydrated samples with filled line patterns.

The PFICE ionomers exhibit larger hydrophilic domain separation (d-spacing) and enhanced local ordering compared to Nafion and the 3M PFSA, and this is likely coupled to the greater water uptake and conductivity in PFICE ionomers. The expanded hydrophilic domains in PFICE-2 and PFICE-3 are clearly seen in the dry membranes as the peaks are at lower q compared to Nafion and the PFSA. The domain spacing, determined from the peak position, of the dry ionomers correlates very well with the size of the side-chain (Figure 7), increasing linearly as a function of estimated side-chain length. This linear trend also holds when comparing the d-spacing to the approximated extended, linear side-chain length (Supporting Information). This implies that side-chain length is a controllable molecular design parameter that can be used to predict ionomer domain spacing. A strong correlation

between inter-domain distance of ionic groups and side-chain length has also been observed for styrene-based ionomers with an ionic group (COO^-) at the end of variable-length side-chains.[78] This suggests that side-chain length can be used to predict degree of phase separation for ionomers with different side-chains. However, the change in domain spacing with side-chain (i.e. slope of d-spacing vs. side-chain length) varies depending on the chemistry of the ionomer side-chain. This is plausible because certain functional groups can alter conformational states of the side-chain and their local water-ion interactions within hydrophilic domains in ionomer membranes, especially under dry or low hydration conditions.

The ionomer membranes all swell when immersed in liquid water, which is evident by the shift in the ionomer peak position to lower q in the presence of water, as shown in Figure 6. Interestingly, PFICE-2 shows the greatest increase in ionomer domain spacing when water is introduced, expanding from 38.0 Å to 54.1 Å (Figure 7). PFICE ionomers with additional hydrophilic bis(sulfonyl)imide groups on the side-chain could absorb more water molecules per ionic group, and per side-chain, which leads to higher macroscopic swelling at a given RH. An important manifestation of this effect is observed especially at low RH levels, with the PFICE ionomers retaining more (residual) water molecules compared to PFSAs. The NEXAFS profiles of PFICE ionomers do not change as significantly when hydrated compared to Nafion and PFSA (Supporting Information), further suggesting that PFICE polymers retain more water even when dry.

Moreover, PFICE ionomers exhibit greater ordering compared to Nafion and the 3M PFSA, which is evidenced by the reduced FWHM of the hydrophilic domain peaks in PFICE-2 and PFICE-3 (Figure 7). Generally, a broader peak (greater FWHM) indicates a larger distribution of domain spacings, and a less ordered nanostructure. Both PFICE-2 and PFICE-3 show similar FWHM values with little change in peak width between dry and hydrated samples. Nafion and 3M PFSA, on the other hand, have larger FWHM values in the hydrated state, which increases further upon dehydration to the dry state. An increase in organizational order (decrease in peak width) with increasing side-chain length has been observed

for styrene-based ionomers.[78] The increased side-chain lengths in PFICE may provide more conformational freedom that allows the ionic groups to organize more easily into ordered domains. Compared to PFSAs, PFICE ionomers exhibit not only stronger local domain order, but also similar structural order between dry and hydrated environments. This latter phenomenon is particularly important as it demonstrates the PFICE ionomer's ability to preserve nano-structural order across various and RH levels. Overall, the qualitative trends in terms of domain spacing and peak width revealed by RXS are also seen in hard X-ray SAXS, as shown in the Supporting Information.

RXS can provide additional insights because the incident X-ray energy can be changed, allowing for elemental sensitivity and tuning of chemical contrast. Scattering profiles at different energies reveal changes in the peak profiles indicative of changes in sensitivity to sulfur-rich domains. To compare the energy-dependent scattering features across the different ionomers, scattering profiles are plotted as Iq^2 vs. q, which gives an experimental approximation of Porod's scattering invariant,[42,43] or the total scattering intensity (TSI). The invariant property of the TSI makes it a useful measure of a domain's overall scattering power, irrespective of the scattering angle of interest (i.e. q) and the size or morphology of the domain.[79,80] The area under the ionomer peak is significantly greater at 2476 eV (close to the S K-edge absorption onset, or"on resonance") compared to 2460 eV (before the absorption edge, or"off resonance") for all the ionomers, revealing an increase in overall scattering power at 2476 eV solely due to enhanced sensitivity to the presence of sulfur (shown in the Supporting Information). The full width at half maximum values of the ionomer peaks for Iq^2 vs. q profiles (FWHM_{Iq2}) collected at 2460 eV and 2476 eV of dry (ambient) PFSA and PFICE materials are shown in Figure 9a and can be used to shed more insight into the distribution of sulfur-rich domains. The PFSA ionomer exhibits an increase in ionomer peak width at 2476 eV compared to 2460 eV (Figure 9a). Scattering contrast at 2460 eV (off resonance) arises mainly due to overall differences in electron density between hydrated and dehydrated domains. At 2476 eV (on resonance), however, greater

contrast can be achieved between domains based on their sulfur content. The increase in FWHM_{Iq2} at 2476 eV seen for the PFSA ionomer suggests that, at this energy, scattering is sensitive to a greater distribution of d-spacings, which includes correlation lengths among sulfur-rich domains with very low water content and sulfur-rich domains with a higher degree of hydration. This is depicted schematically for the PFSA sample in the top row of Figure 9b. In contrast to PFSA, PFICE ionomer peak widths remain nearly constant between these two energies (Figure 9a), indicating that PFICE membranes under dry (ambient) conditions contain a more homogeneous distribution of sulfur-rich domains with fewer regions of very low water content. This is illustrated in Figure 9b. This may also partially explain why PFICE membranes maintain local order, e.g. similar peak widths, between dry (ambient) and wet conditions (Figure 7).

The unique chemistry and side-chain lengths of the PFICE ionomers imparts a nano-morphology with larger and better dispersed domains that enhance local order of the hydrophilic phase, which is accompanied by a higher number of water molecules per ionic group for a given RH. Moreover, this ordering is maintained in both low and high hydration states and could be a morphological signature of ionomers with improved transport properties across a range of relative humidity values. The combined effects of a multi-acid side-chain and ordered domain network leading to improved conductivity for PFICE ionomers is illustrated in Figure 10. The higher water-uptake capacity of PFICE ionomers, especially at low RH, along with their ability to retain their phase-separated morphology, is of great importance due to their potential benefits for dry-hot operations. Furthermore, side-chain length and chemistry can be correlated with the phase separated nano-structure and conductivity, opening new avenues for tuning materials chemistry to control and optimize transport.

3.4 Connecting morphology and chemistry

Combining molecular-level details regarding bonding and proton dissociation determined by theory-guided spectroscopy with insights into morphology from scattering can provide useful

information to elucidate the origins of conductivity. The scattering peak profiles at energies on and off resonance suggest that PFSA ionomer membranes under ambient conditions may comprise of some sulfonic acid-containing phases with very low hydration. The NEXAFS spectra of PFSA exhibits a low-energy shoulder at around 2478.5 eV, and the main absorption feature peaks near 2479.7 eV. DFT-computed NEXAFS spectra of PFSA with zero, one and three added water molecules show that the lowest energy peak (2478.3 eV) and the peak at 2480 eV are contributions from the lower hydration states (zero and one added water), as shown in Figure 8a. Conversely, the low-energy shoulder, indicative of a very low hydration state, is not present in the experimental NEXAFS spectra of PFICE-2 (Figure 8b). This supports the previously discussed energy-dependent scattering profiles implying that PFICE membranes in low RH maintain a more spatially uniform hydration state with fewer ionic domains of very low water content.

PFICE-2 and PFICE-3 exhibit similar conductivity as a function of λ, but PFICE-2 has moderately higher conductivity compared to PFICE-3, especially at low- and mid-level RH, where local chemistry effects are more influential on proton dissociation and transfer (Figure 3 and 10). Their conductivity becomes comparable at high RH values, which suggests their similar mesoscale hydrated morphology dominates conductivity. PFICE-2 and PFICE-3 show generally similar domain network features based on scattering, although the domain spacing in PFICE-2 expands more than PFICE-3 when hydrated (Figure 7). This suggests subtle chemistry differences could play a role in nano-swelling of domains and overall conductivity. Modeling and simulation studies have shown that electrostatic interactions within polymer-bound anionic groups and cation solvation energy have the greatest impact on charge migration at the molecular and domain-scale, and this is influenced by the chemistry and resulting charge delocalization on the side-chain.[68,74] Previous work has shown that the proximity of protogenic groups and the charge delocalization on the side-chain are important factors that dictate hydrogen bonding and proton dissociation at low hydration levels.[68] PFICE ionomers have a side-chain chemistry and combination of protogenic groups

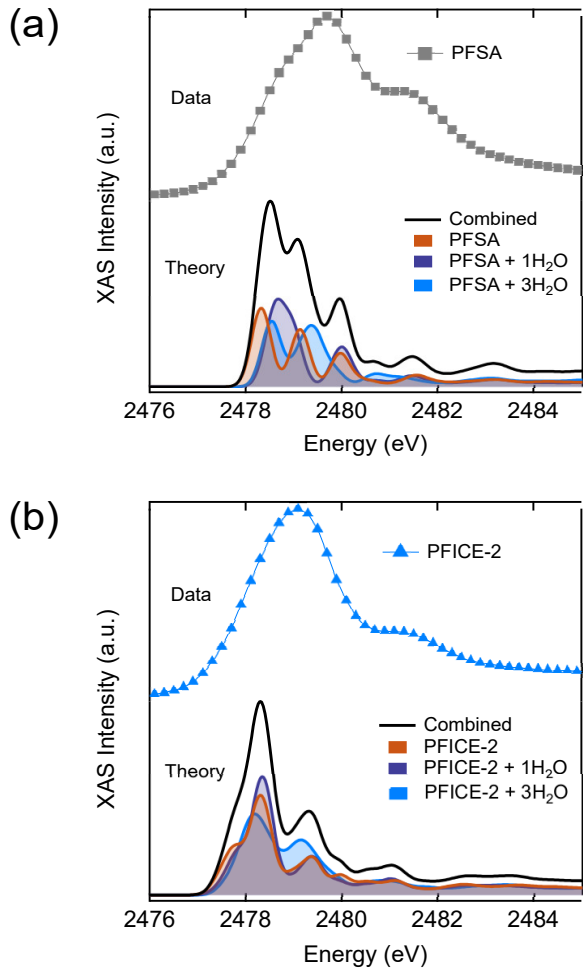

Figure 8: Sulfur K-edge transmission NEXAFS data of dry (ambient) PFSA and PFICE-2 ionomers compared to simulated spectra with zero, one or three added water molecules. The PFSA ionomer is shown in (a) and the water molecules hydrogen bond to the sulfonic acid group. A similar comparison for PFICE-2 is shown in (b). The calculated spectra of one added water is an average two configurations: a water molecule at the sulfonic acid group and a water molecule at the bis(sulfonyl)imide group. The simulated spectra with three added water molecules is an average of three different configurations: water molecules bridging the sulfonic acid and bis(sulfonyl)imide group, surrounding the sulfonic acid group, or surrounding the bis(sulfonyl)imide group (as shown in Figure 5c).

that facilitates water hydrogen bonding configurations promoting proton dissociation, as illustred in Figure 10. The longer side-chain on PFICE-3 allows for more conformational freedom compared to PFICE-2 that may increase the variability in the relative distances and orientations among the sulfonic acid group and the two bis(sulfonyl)imide groups and influence proton dissociation.

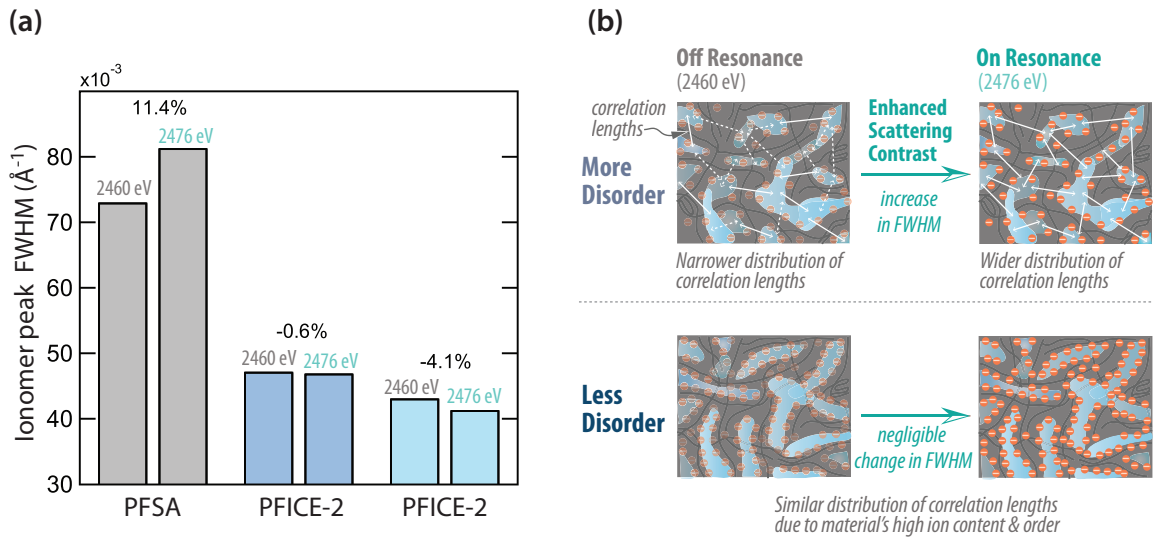

Figure 9: Peak width ($FWHM_{Iq2}$) determined from Iq^2 vs q data of the ionomer peaks as a function of incident X-ray energy is shown in (a). $FWHM_{Iq2}$ values for a given material are from the same sample. Data presented is for dry (ambient) membranes. Schematic illustrating changes in contrast for the two different energies is shown in (b). For more disordered ionomers, such as PFSA (top left), the distribution of length-scales contributing to the peak width are likely due to distances between hydrated domains (shown by solid arrows). Off resonance (2460 eV) scattering does not capture some of the correlation lengths (shown by dashed arrows) due to low contrast from sulfur-rich domains with very low water content in PFSA. However, scattering contrast from these domains is enhanced on resonance (at 2476 eV, top right image), which leads to a greater distribution of length-scales resulting in a broader scattering peak (larger FWHM) at this energy. For PFICE ionomers (bottom row), the higher residual water and stronger local order result in a similar distribution of length-scales (and FWHM values) both at off resonance and on resonance energies.

A clearer picture of ion transport in disordered ionomers emerges from spectroscopic and structural insights. While energy-dependent X-ray scattering and spectroscopy cannot directly probe the connectivity of nano-domains, it provides improved understanding of the interplay between the chemical interactions within the ionic moieties and nano-morphology. A number of experimental and modeling studies indicate that a continuous transport pathway with less clustering of domains could reduce tortuosity and be preferred for ion-conducting polymers.[81–87] The findings presented here provide indirect evidence of the role of mesoscale effects in enhancing the conductivity of PFICE ionomers where locally-flat domains with better local order and interconnectivity form (Figure 10). In such a structure, the number of isolated, discrete domains could be reduced in favor of a less tortuous transport pathway, and

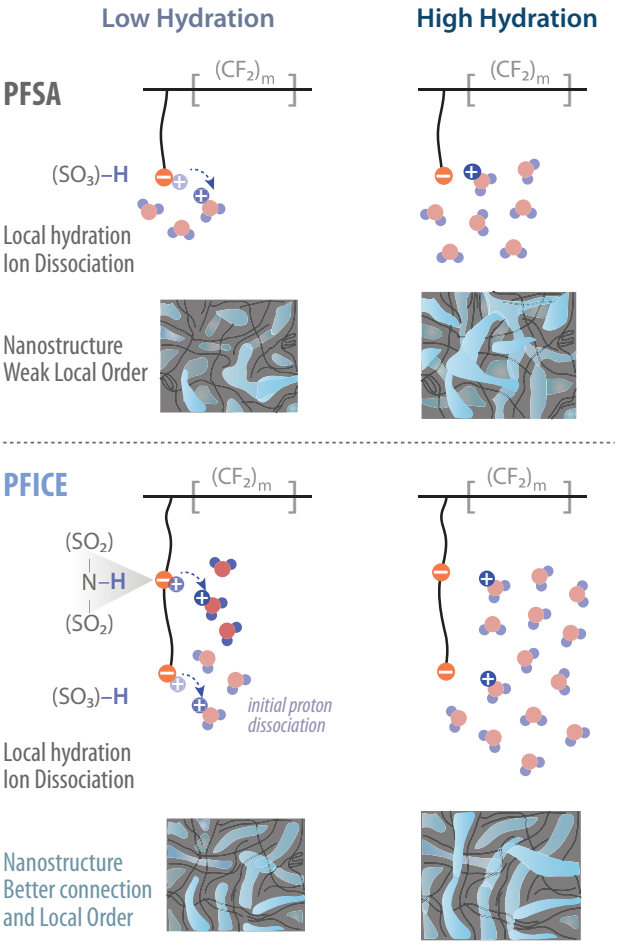

Figure 10: Pictorial description of the impact of side-chain chemistry on local environment and nanostructure, including proton dissociation with hydration and associated changes in local-order of hydrophilic domains, based on simulated NEXAFS results and scattering data.

this would lead to greater short-range order and more well-defined scattering peaks. In addition, reducing the EW, or backbone length, has been shown to mitigate strong aggregation of ionic domains and improve connectivity.[21,88–90] The data presented here indicate that adding acid groups on the side-chain without changing m_{TFE} could effectively reduce EW and lead not only to greater water network connectivity, but also a more continuous hydrogen-bonded water structure with enhanced charge delocalization. This is in agreement with previous descriptions of ion transport in PFSAs,[1,91–94] and PFIAs.[68,72] The length-scales probed in this study could be integrated with other complementary techniques such as NMR,[94,95] which could delineate the ion mobility and water diffusion in multi-acid side-chain ionomers. NMR

studies on PFSAs have shown that self-diffusion of water along with relaxation times could be used to probe water transport mechanisms at intermediate length-scales,[93,95–98] and this could provide additional information on the role of morphology.

The results presented herein focus on characterization of membranes with varying hydration levels at room temperature, but polymer-electrolyte fuel cells typically operate around 80 °C. It was shown recently that the increase in conductivity with the number of protogenic groups per side-chain is more pronounced at 80 °C.[11] Increased segmental motion of chains and higher ion mobility at higher temperatures influence proton dissociation and transport, highlighting the importance of future NEXAFS and RXS studies at elevated temperatures combined with finite-temperature calculations, for example, simulations incorporating molecular dynamics.

Advances in polymer synthesis can create materials with precise placement of ionic groups that could improve control over ion transport. Precise or nearly precise acid containing polymers, for example, linear polyethylene with sulfonic acid groups along the side-chain, exhibit transport domains of well-defined size and ordered morphologies.[99,100] Although precise sulfonated polyethylene exhibits a higher proton conductivity than Nafion, the conductivity is comparable to PFICE ionomers despite its greater long-range order. Nevertheless, polymers with precise or nearly precise placement of ionic functional groups are promising systems not only for developing detailed structure-property relationships, but also for unraveling the role of structural order in transport. Highly-ordered morphologies that produce strong scattering signals allow X-ray methods to more easily determine features such as the distribution of specific functional groups or their orientation, underscoring the need for advanced X-ray techniques that connect morphology and chemistry going forward.

4 Conclusions

Ion-conducting polymers that can transport protons under hot and dry conditions are needed for advancements in polymer-electrolyte fuel cells and other electrochemical energy applications. This requires new ionomer chemistries that provide control over proton dissociation and a suitable phase-separated morphology for optimized ion conductivity, without sacrificing stability. Perfluoro Ionene Chain Extended (PFICE) ionomers with a tunable number of protogenic bis(sulfonyl)imide groups on the side-chain show greater water uptake and improved proton conductivity over a range of relative humidity values compared to typical perfluorosulfonic acid (PFSA) ionomers, including Nafion. Importantly, PFICE ionomers that share the same backbone length between side-chains with PFSAs, exhibit higher ion conductivity for the same hydration level per ionic group.

PFICE ionomers exhibit enhanced conductivity due to not only greater water uptake, but also a combined impact of chemical interactions governing proton dissociation with water and more efficient proton transport. In particular, tunable acid content via side-chain modification enables control over local proton-water hydrogen bonding interactions, which has strong implications for optimizing dissociation and transport over a range of hydration levels. The multi-acid side-chains in PFICE ionomers are the chemical origin of its phase-separated morphology with improved short-range order among hydrophilic nano-domains in both dry and wet conditions. This results in higher conductivity, especially at low relative humidity values, compared to a PFSA ionomer with the same fluorocarbon backbone. X-ray absorption spectroscopy guided by first-principles calculations reveals distinct sulfur bonding environments in the different ionic groups and showcases the potential to distinguish among various degrees of hydration and hydration configurations. Notably, core-level absorption spectra of PFSA under dry ambient conditions shows contributions from phases with very low water content that is not clearly evident in PFICE. This supports the greater measured residual water content in PFICE compared to PFSA. Furthermore, molecular models suggest that compared to PFSA, PFICE ionomers have a side-chain chemistry that promotes

hydrogen bonding configurations of water that facilitate proton dissociation.

While an interconnected phase-separated morphology is critical to ionomer membranes' macroscopic transport, nano and mesoscale chemical heterogeneities each play significant roles, which could be delineated by a combination of *in situ* spectroscopic and scattering techniques. Energy-tunable X-rays are well-suited for decoupling the impacts of chemistry and morphology across these length-scales, especially when X-ray absorption spectroscopy calculations and measurements are combined with resonant scattering near relevant elemental edges (e.g. sulfur) to probe these materials in realistic *in situ* environmental conditions. In this work, we report that resonant X-ray scattering reveals a phase-separated morphology with improved short-range order in the PFICE ionomers, where the ionomer side-chain length and acidity are strongly correlated to hydrophilic domain separation distance, particularly in dry (ambient) membranes. PFICE ionomers exhibit greater local ordering, which is maintained in both low and high hydration levels. Furthermore, scattering profiles at different energies near the sulfur absorption edge suggest that the PFSA ionomers may have minimally hydrated sulfur-rich domains in ambient conditions with a distribution of d-spacings that is difficult to detect without resonant scattering. Overall, this highlights the importance of elementally sensitive techniques that are well-suited for characterizing membranes in device-relevant geometries and environments.

In general, these correlations among chemistry, phase-separated morphology, and transport in ionomer membranes enable fundamental structure-property-function relationships that will drive the design of next-generation ionomers and other functional soft materials for energy and environmental applications.

Acknowledgement

Authors would like to thank Jessica Luo and Andrew Crothers for insights and supplemental work. Authors would also thank Andrew Haug of 3M for helpful discussion. Also special

thanks to David Kilcoyne for assistance in designing sample holders for *in situ* measurements, and Chenhui Zhu and Eric Schaible for their assistance with facilitating the hard X-ray scattering experiments at the Advanced Light Source (ALS) beamline 7.3.3. AK acknowledges support from the Assistant Secretary for Energy Efficiency and Renewable Energy, Fuel Cell Technologies Office under contract no. DE-AC02-05CH11231. GMS, IAC, JF, and CW acknowledge support from the Advanced Light Source. The use of the Advanced Light Source (ALS) including beamlines 5.3.1 (resonant X-ray scattering and spectroscopy at the sulfur K-edge), 7.3.3 (hard X-ray SAXS/WAXS) and 11.0.1.2 (soft X-ray absorption spectroscopy), a user project at The Molecular Foundry and use of its computer cluster Etna managed by the High Performance Computing Services Group, and the use of the National Energy Research Scientific Computing (NERSC) Center were performed at Lawrence Berkeley National Laboratory, which is supported by the Director, Office of Science, Office of Basic Energy Sciences, of the DOE under contract No. DE-AC02-05CH11231. Some preliminary resonant X-ray scattering measurements were performed under proposal number 2017G709 on beamline 15A2 at the Photon Factory, Japan and the authors thank Hiroshi Okuda for generous support of these experiments.

Supporting Information Available

Additional simulation and characterization data are provided in the Supporting Information.

References

(1) Kusoglu, A.; Weber, A. Z. New Insights into Perfluorinated Sulfonic-Acid Ionomers. *Chem. Rev.* **2017**, *117*, 987–1104.

(2) Hamrock, S. J.; Yandrasits, M. A. Proton Exchange Membranes for Fuel Cell Applications. *J. Macromol. Sci. Polymer Rev.* **2006**, *46*, 219–244.

(3) Kusoglu, A.; Cho, K. T.; Prato, R. A.; Weber, A. Z. Structural and transport properties of Nafion in hydrobromic-acid solutions. *Solid State Ionics* **2013**, *252*, 68 – 74, SSPC-16 Conference Proceedings SSI Special Issue.

(4) Perry, M. L.; Weber, A. Z. Advanced Redox-Flow Batteries: A Perspective. *J. Electrochem. Soc.* **2016**, *163*, A5064–A5067.

(5) Weber, A. Z.; Mench, M. M.; Meyers, J. P.; Ross, P. N.; Gostick, J. T.; Liu, Q. Redox flow batteries: a review. *J. Appl. Electrochem.* **2011**, *41*, 1137.

(6) Modestino, M. A.; Walczak, K. A.; Berger, A.; Evans, C. M.; Haussener, S.; Koval, C.; Newman, J. S.; Ager, J. W.; Segalman, R. A. Robust production of purified H_2 in a stable, self-regulating, and continuously operating solar fuel generator. *Energy Environ. Sci.* **2014**, *7*, 297–301.

(7) Rodriguez, C. A.; Modestino, M. A.; Psaltis, D.; Moser, C. Design and cost considerations for practical solar-hydrogen generators. *Energy Environ. Sci.* **2014**, *7*, 3828–3835.

(8) Hickner, M. A. Ion-containing polymers: new energy & clean water. *Materials Today* **2010**, *13*, 34 – 41.

(9) Mauritz, K. A.; Moore, R. B. State of Understanding of Nafion. *Chem. Rev.* **2004**, *104*, 4535–4586.

(10) Kusoglu, A.; Dursch, T. J.; Weber, A. Z. Nanostructure/Swelling Relationships of Bulk and Thin-Film PFSA Ionomers. *Adv. Funct. Mater.* **2016**, *26*, 4961–4975.

(11) Yandrasits, M.; Lindell, M.; Schaberg, M.; Kurkowski, M. Increasing Fuel Cell Efficiency by Using Ultra-Low Equivalent Weight Ionomers. *Electrochem. Soc. Interface* **2017**, *26*, 49–53.

(12) Hamrock, S. J.; Herring, A. M. In *Encyclopedia of Sustainability Science and Technology*; Meyers, R. A., Ed.; Springer New York: New York, NY, 2012; pp 8328–8347.

(13) Schaberg, M. S.; Abulu, J. E.; Haugen, G. M.; Emery, M. A.; O'Conner, S. J.; Xiong, P. N.; Hamrock, S. New Multi Acid Side-Chain Ionomers for Proton Exchange Membrane Fuel Cells. *ECS Trans.* **2010**, *33*, 627–633.

(14) Kongkanand, A.; Mathias, M. F. The Priority and Challenge of High-Power Performance of Low-Platinum Proton-Exchange Membrane Fuel Cells. *J. Phys. Chem. Lett* **2016**, *7*, 1127–1137.

(15) Yandrasits, M.; Lindell, M.; Peppin, D.; Komlev, A.; Hamrock, S.; Haugen, G.; Fort, E.; Kalstabakken, K. Chemical Stability of Perfluorobis(sulfonyl)imide-Acid (PFIA) Ionomers in Open Circuit Voltage (OCV) Accelerated Test Conditions. *J. Electrochem. Soc.* **2018**, *165*, F3261–F3270.

(16) Weber, A. Z.; Kusoglu, A. Unexplained transport resistances for low-loaded fuel-cell catalyst layers. *J. Mater. Chem. A* **2014**, *2*, 17207–17211.

(17) Puskar, L.; Ritter, E.; Schade, U.; Yandrasits, M.; Hamrock, S. J.; Schaberg, M.; Aziz, E. F. Infrared dynamics study of thermally treated perfluoroimide acid proton exchange membranes. *Phys. Chem. Chem. Phys.* **2017**, *19*, 626–635.

(18) Economou, N. J.; Barnes, A. M.; Wheat, A. J.; Schaberg, M. S.; Hamrock, S. J.; Buratto, S. K. Investigation of Humidity Dependent Surface Morphology and Proton Conduction in Multi-Acid Side Chain Membranes by Conductive Probe Atomic Force Microscopy. *J. Phys. Chem. B* **2015**, *119*, 14280–14287.

(19) Bawagan, A.; Hamrock, S.; Schaberg, M.; Yousef, I.; Ritter, E.; Schade, U. Far-infrared studies on Nafion and perfluoroimide acid (PFIA) and their alkali salts. *Vib. Spectrosc.* **2014**, *75*, 213 – 217.

(20) Danilczuk, M.; Lancucki, L.; Schlick, S.; Hamrock, S. J.; Haugen, G. M. In-Depth Profiling of Degradation Processes in a Fuel Cell: 2D Spectral-Spatial FTIR Spectra of Nafion Membranes. *ACS Macro Lett.* **2012**, *1*, 280–285.

(21) Clark II, J. K.; Paddison, S. J.; Hamrock, S. J. The effect of hydrogen bond reorganization and equivalent weight on proton transfer in 3M perfluorosulfonic acid ionomers. *Phys. Chem. Chem. Phys.* **2012**, *14*, 16349–16359.

(22) Danilczuk, M.; Lin, L.; Schlick, S.; Hamrock, S. J.; Schaberg, M. S. Understanding the fingerprint region in the infra-red spectra of perfluorinated ionomer membranes and corresponding model compounds: Experiments and theoretical calculations. *J. Power Sources* **2011**, *196*, 8216 – 8224.

(23) Emery, M.; Frey, M.; Guerra, M.; Haugen, G.; Hintzer, K.; Lochhaas, K. H.; Pham, P.; Pierpont, D.; Schaberg, M.; Thaler, A.; Yandrasits, M.; Hamrock, S. The Development of New Membranes for Proton Exchange Membrane Fuel Cells. *ECS Trans.* **2007**, *11*, 3–14.

(24) Yandrasits, M.; Lindell, M.; Komlev, A.; Fort, E.; Hamrock, S.; Peppin, D. M.; Kalstabakken, K. Stability of Perfluoro Bis(Sulfonyl)Imide-Based Ionomers in Fuel Cell Membranes and Electrodes. *ECS Trans.* **2018**, *86*, 381–394.

(25) Stöhr, J. *NEXAFS Spectroscopy*; Springer Series in Surface Sciences; Springer, 1992.

(26) Watts, B.; Swaraj, S.; Nordlund, D.; Lüning, J.; Ade, H. Calibrated NEXAFS spectra of common conjugated polymers. *J. Chem. Phys.* **2011**, *134*.

(27) Meshot, E. R.; Zwissler, D. W.; Bui, N.; Kuykendall, T. R.; Wang, C.; Hexemer, A.; Wu, K. J. J.; Fornasiero, F. Quantifying the Hierarchical Order in Self-Aligned Carbon Nanotubes from Atomic to Micrometer Scale. *ACS Nano* **2017**, *11*, 5405–5416.

(28) Abberley, J. P.; Killah, R., RossWalker; Storey, J. M. D.; Imrie, C. T.; Salamoczyk, M.; Zhu, C.; Gorecka, E.; Pociecha, D. Heliconical smectic phases formed by achiral molecules. *Nat. Commun.* **2018**, *9*.

(29) Zhu, C.; Tuchband, M. R.; Young, A.; Shuai, M.; Scarbrough, A.; Walba, D. M.; Maclennan, J. E.; Wang, C.; Hexemer, A.; Clark, N. A. Resonant Carbon K-Edge Soft X-Ray Scattering from Lattice-Free Heliconical Molecular Ordering: Soft Dilative Elasticity of the Twist-Bend Liquid Crystal Phase. *Phys. Rev. Lett.* **2016**, *116*, 147803.

(30) Zhu, C.; Wang, C.; Young, A.; Liu, F.; Gunkel, I.; Chen, D.; Walba, D.; Maclennan, J.; Clark, N.; Hexemer, A. Probing and Controlling Liquid Crystal Helical Nanofilaments. *Nano Lett.* **2015**, *15*, 3420–3424.

(31) Ye, D.; Le, T.; Wang, C.; Zwart, P. H.; Zhu, C.; Gomez, E. W.; Gomez, E. D. Resonant Soft X-Ray Scattering of Proteins in Solution. *Biophys. J.* **2018**, *114*, 370a.

(32) Ingham, B.; Smialowska, A.; Kirby, N. M.; Wang, C.; Carr, A. J. A structural comparison of casein micelles in cow, goat and sheep milk using X-ray scattering. *Soft Matter* **2018**, *14*, 3336–3343.

(33) Su, G. M.; Cordova, I. A.; Brady, M. A.; Prendergast, D.; Wang, C. Combining theory and experiment for X-ray absorption spectroscopy and resonant X-ray scattering characterization of polymers. *Polymer* **2016**, *99*, 782 – 796.

(34) Ade, H.; Hitchcock, A. P. NEXAFS microscopy and resonant scattering: Composition and orientation probed in real and reciprocal space. *Polymer* **2008**, *49*, 643 – 675.

(35) Liu, F.; Brady, M. A.; Wang, C. Resonant Soft X-ray Scattering for Polymer Materials. *Eur. Polym. J.* **2016**, *81*, 555–568.

(36) Culp, T. E.; Ye, D.; Paul, M.; Roy, A.; Behr, M. J.; Jons, S.; Rosenberg, S.; Wang, C.; Gomez, E. W.; Kumar, M.; Gomez, E. D. Probing the Internal Microstructure of Polyamide Thin-Film Composite Membranes Using Resonant Soft X-ray Scattering. *ACS Macro Lett.* **2018**, *7*, 927–932.

(37) Virgili, J. M.; Tao, Y.; Kortright, J. B.; Balsara, N. P.; Segalman, R. A. Analysis of Order Formation in Block Copolymer Thin Films Using Resonant Soft X-ray Scattering. *Macromolecules* **2007**, *40*, 2092–2099.

(38) Litofsky, J. H.; Lee, Y.; Aplan, M. P.; Kuei, B.; Hexemer, A.; Wang, C.; Wang, Q.; Gomez, E. D. Polarized Soft X-ray Scattering Reveals Chain Orientation within Nanoscale Polymer Domains. *Macromolecules* **2019**, *52*, 2803–2813.

(39) Coric, M.; Saxena, N.; Pflüger, M.; Müller-Buschbaum, P.; Krumrey, M.; Herzig, E. M. Resonant Grazing-Incidence Small-Angle X-ray Scattering at the Sulfur K-Edge for Material-Specific Investigation of Thin-Film Nanostructures. *J. Phys. Chem. Lett.* **2018**, *9*, 3081–3086.

(40) Gann, E.; Young, A. T.; Collins, B. A.; Yan, H.; Nasiatka, J.; Padmore, H. A.; Ade, H.; Hexemer, A.; Wang, C. Soft x-ray scattering facility at the Advanced Light Source with real-time data processing and analysis. *Rev. Sci. Instrum.* **2012**, *83*, 045110.

(41) Ravel, B.; Newville, M. *ATHENA*, *ARTEMIS*, *HEPHAESTUS*: data analysis for X-ray absorption spectroscopy using *IFEFFIT*. *J. Synchrotron Rad.* **2005**, *12*, 537–541.

(42) Porod, G. Die Röntgenkleinwinkelstreuung von dichtgepackten kolloiden Systemen. II. Teil. *Kolloid-Zeitschrift* **1952**, *125*, 108–122.

(43) Roe, R.-J. *Methods of X-ray and Neutron Scattering in Polymer Science*; Oxford University Press, 2000.

(44) Kusoglu, A.; Savagatrup, S.; Clark, K. T.; Weber, A. Z. Role of Mechanical Factors in Controlling the Structure-Function Relationship of PFSA Ionomers. *Macromolecules* **2012**, *45*, 7467–7476.

(45) Perdew, J. P.; Burke, K.; Ernzerhof, M. Generalized Gradient Approximation Made Simple. *Phys. Rev. Lett.* **1996**, *77*, 3865–3868.

(46) Vanderbilt, D. Soft self-consistent pseudopotentials in a generalized eigenvalue formalism. *Phys. Rev. B* **1990**, *41*, 7892–7895.

(47) Prendergast, D.; Galli, G. X-Ray Absorption Spectra of Water from First Principles Calculations. *Phys. Rev. Lett.* **2006**, *96*, 215502.

(48) Hohenberg, P.; Kohn, W. Inhomogeneous Electron Gas. *Phys. Rev.* **1964**, *136*, B864.

(49) Kohn, W.; Sham, L. J. Self-Consistent Equations Including Exchange and Correlation Effects. *Phys. Rev.* **1965**, *140*, A1133.

(50) Cohen, A. J.; Mori-Sánchez, P.; Yang, W. Fractional charge perspective on the band gap in density-functional theory. *Phys. Rev. B* **2008**, *77*, 115123.

(51) Mori-Sánchez, P.; Cohen, A. J.; Yang, W. Localization and Delocalization Errors in Density Functional Theory and Implications for Band-Gap Prediction. *Phys. Rev. Lett.* **2008**, *100*, 146401.

(52) Becke, A. D. A new mixing of HartreeFock and local densityfunctional theories. *J. Chem. Phys.* **1993**, *98*, 1372–1377.

(53) Aryasetiawan, F.; Gunnarsson, O. TheGWmethod. *Rep. Prog. Phys.* **1998**, *61*, 237–312.

(54) Hedin, L. New Method for Calculating the One-Particle Green's Function with Application to the Electron-Gas Problem. *Phys. Rev.* **1965**, *139*, A796–A823.

(55) Pascal, T. A.; Wujcik, K. H.; Velasco-Velez, J.; Wu, C.; Teran, A. A.; Kapilashrami, M.; Cabana, J.; Guo, J.; Salmeron, M.; Balsara, N.; Prendergast, D. X-ray Absorption Spectra of Dissolved Polysulfides in LithiumSulfur Batteries from First-Principles. *J. Phys. Chem. Lett.* **2014**, *5*, 1547–1551, PMID: 26270094.

(56) Kusoglu, A.; Weber, A. Z. *Polymers for Energy Storage and Delivery: Polyelectrolytes for Batteries and Fuel Cells*; 2012; Chapter 11, pp 175–199.

(57) Shi, S.; Weber, A. Z.; Kusoglu, A. Structure-Transport Relationship of Perfluorosulfonic-Acid Membranes in Different Cationic Forms. *Electrochim. Acta* **2016**, *220*, 517 – 528.

(58) Cooper, K. R. Progress Toward Accurate Through-Plane Ion Transport Resistance Measurement of Thin Solid Electrolytes. *J. Electrochem. Soc.* **2010**, *157*, B1731–B1739.

(59) Yan, Z. B.; Hayes, R.; Melo, L. G. A.; Goward, G. R.; Hitchcock, A. P. X-ray Absorption and Solid-State NMR Spectroscopy of Fluorinated Proton Conducting Polymers. *J. Phys. Chem. C* **2018**, *122*, 3233–3244.

(60) Isegawa, K.; Nagami, T.; Jomori, S.; Yoshida, M.; Kondoh, H. *In situ* S-K XANES study of polymer electrolyte fuel cells: changes in the chemical states of sulfonic groups depending on humidity. *Phys. Chem. Chem. Phys.* **2016**, *18*, 25183–25190.

(61) Vijayakumar, M.; Govind, N.; Li, B.; Wei, X.; Nie, Z.; Thevuthasan, S.; Sprenkle, V.; Wang, W. Aqua-Vanadyl Ion Interaction with Nafion Membranes. *Front. Energy Res.* **2015**, *3*, 10.

(62) Wang, C.; Lee, D. H.; Hexemer, A.; Kim, M. I.; Zhao, W.; Hasegawa, H.; Ade, H.; Russell, T. P. Defining the Nanostructured Morphology of Triblock Copolymers Using Resonant Soft X-ray Scattering. *Nano Lett.* **2011**, *11*, 3906–3911.

(63) Damian Risberg, E.; Eriksson, L.; Mink, J.; Pettersson, L. G. M.; Skripkin, M. Y.; Sandström, M. Sulfur X-ray Absorption and Vibrational Spectroscopic Study of Sulfur Dioxide, Sulfite, and Sulfonate Solutions and of the Substituted Sulfonate Ions $X_3CSO_3^-$ (X = H, Cl, F). *Inorg. Chem.* **2007**, *46*, 8332–8348.

(64) Patel, S. N.; Su, G. M.; Luo, C.; Wang, M.; Perez, L. A.; Fischer, D. A.; Prendergast, D.; Bazan, G. C.; Heeger, A. J.; Chabinyc, M. L.; Kramer, E. J. NEXAFS Spec-

troscopy Reveals the Molecular Orientation in Blade-Coated Pyridal[2,1,3]thiadiazole-Containing Conjugated Polymer Thin Films. *Macromolecules* **2015**, *48*, 6606–6616.

(65) Su, G. M.; Patel, S. N.; Pemmaraju, C. D.; Prendergast, D.; Chabinyc, M. L. First-Principles Predictions of Near-Edge X-ray Absorption Fine Structure Spectra of Semiconducting Polymers. *J. Phys. Chem. C* **2017**, *121*, 9142–9152.

(66) Rundel, K.; Liang, Y.; Welford, A.; Prendergast, D.; McNeill, C. R. Understanding the effect of thionation on naphthalene diimide using first-principles predictions of near-edge x-ray absorption fine structure spectra. *J. Chem. Phys.* **2019**, *150*, 104302.

(67) Yan, L.; Balbuena, P. B.; Seminario, J. M. Perfluorobutane sulfonic acid hydration and interactions with O_2 adsorbed on Pt_3. *J. Phys. Chem. A* **2006**, *110*, 4574–4581.

(68) II, J. K. C.; Paddison, S. J. Proton dissociation and transfer in proton exchange membrane ionomers with multiple and distinct pendant acid groups: An ab initio study. *Electrochim. Acta* **2013**, *101*, 279 – 292.

(69) Paddison, S. J.; Elliott, J. A. The effects of backbone conformation on hydration and proton transfer in the short-side-chain perfluorosulfonic acid membrane. *Solid State Ionics* **2006**, *177*, 2385 – 2390, Solid State Ionics 15: Proceedings of the 15th International Conference on Solid State Ionics, Part II.

(70) Paddison, S. J.; Elliott, J. A. On the consequences of side chain flexibility and backbone conformation on hydration and proton dissociation in perfluorosulfonic acid membranes. *Phys. Chem. Chem. Phys.* **2006**, *8*, 2193–2203.

(71) Paddison, S. J.; Elliott, J. A. Molecular Modeling of the Short-Side-Chain Perfluorosulfonic Acid Membrane. *J. Phys. Chem. A* **2005**, *109*, 7583–7593.

(72) Idupulapati, N.; Devanathan, R.; Dupuis, M. Ab Initio Study of Hydration and Proton Dissociation in Ionomer Membranes. *J. Phys. Chem. A* **2010**, *114*, 6904–6912.

(73) Koppel, I. A.; Taft, R. W.; Anvia, F.; Zhu, S.-Z.; Hu, L.-Q.; Sung, K.-S.; DesMarteau, D. D.; Yagupolskii, L. M.; Yagupolskii, Y. L. a. The Gas-Phase Acidities of Very Strong Neutral Bronsted Acids. *J. Am. Chem. Soc.* **1994**, *116*, 3047–3057.

(74) Crothers, A. R.; Radke, C. J.; Weber, A. Z. Impact of Nano- and Mesoscales on Macroscopic Cation Conductivity in Perfluorinated-Sulfonic-Acid Membranes. *J. Phys. Chem. C* **2017**, *121*, 28262–28274.

(75) Elliott, J. A.; Wu, D.; Paddison, S. J.; Moore, R. B. A unified morphological description of Nafion membranes from SAXS and mesoscale simulations. *Soft Matter* **2011**, *7*, 6820–6827.

(76) Liu, Y.; Horan, J. L.; Schlichting, G. J.; Caire, B. R.; Liberatore, M. W.; Hamrock, S. J.; Haugen, G. M.; Yandrasits, M. A.; Seifert, S.; Herring, A. M. A Small-Angle X-ray Scattering Study of the Development of Morphology in Films Formed from the 3M Perfluorinated Sulfonic Acid Ionomer. *Macromolecules* **2012**, *45*, 7495–7503.

(77) Sambasivarao, S. V.; Liu, Y.; Horan, J. L.; Seifert, S.; Herring, A. M.; Maupin, C. M. Enhancing Proton Transport and Membrane Lifetimes in Perfluorosulfonic Acid Proton Exchange Membranes: A Combined Computational and Experimental Evaluation of the Structure and Morphology Changes Due to $H_3PW_{12}O_{40}$ Doping. *J. Phys. Chem. C* **2014**, *118*, 20193–20202.

(78) Moore, R. B.; Bittencourt, D.; Gauthier, M.; Williams, C. E.; Eisenberg, A. Small-angle x-ray scattering investigations of ionomers with variable-length side chains. *Macromolecules* **1991**, *24*, 1376–1382.

(79) Collins, B. A.; Li, Z.; Tumbleston, J. R.; Gann, E.; McNeill, C. R.; Ade, H. Absolute Measurement of Domain Composition and Nanoscale Size Distribution Explains Performance in PTB7:$PC_{71}BM$ Solar Cells. *Adv. Energy Mater.* **2012**, *3*, 65–74.

(80) Ferron, T.; Pope, M.; Collins, B. A. Spectral Analysis for Resonant Soft X-Ray Scattering Enables Measurement of Interfacial Width in 3D Organic Nanostructures. *Phys. Rev. Lett.* **2017**, *119*, 167801.

(81) Feng, S.; Savage, J.; Voth, G. A. Effects of Polymer Morphology on Proton Solvation and Transport in Proton-Exchange Membranes. *J. Phys. Chem. C* **2012**, *116*, 19104–19116.

(82) Beers, K. M.; Balsara, N. P. Design of Cluster-free Polymer Electrolyte Membranes and Implications on Proton Conductivity. *ACS Macro Lett.* **2012**, *1*, 1155–1160.

(83) Park, M. J.; Balsara, N. P. Anisotropic Proton Conduction in Aligned Block Copolymer Electrolyte Membranes at Equilibrium with Humid Air. *Macromolecules* **2010**, *43*, 292–298.

(84) Peckham, T. J.; Holdcroft, S. StructureMorphologyProperty Relationships of NonPerfluorinated ProtonConducting Membranes. *Adv. Mater.* **2010**, *22*, 4667–4690.

(85) Chang, Y.; Brunello, G. F.; Fuller, J.; Disabb-Miller, M. L.; Hawley, M. E.; Kim, Y. S.; Hickner, M. A.; Jang, S. S.; Bae, C. Polymer electrolyte membranes based on poly(arylene ether sulfone) with pendant perfluorosulfonic acid. *Polym. Chem.* **2013**, *4*, 272–281.

(86) Chang, Y.; Mohanty, A. D.; Smedley, S. B.; Abu-Hakmeh, K.; Lee, Y. H.; Morgan, J. E.; Hickner, M. A.; Jang, S. S.; Ryu, C. Y.; Bae, C. Effect of Superacidic Side Chain Structures on High Conductivity Aromatic Polymer Fuel Cell Membranes. *Macromolecules* **2015**, *48*, 7117–7126.

(87) Wang, C.; Paddison, S. J. Mesoscale modeling of hydrated morphologies of sulfonated polysulfone ionomers. *Soft Matter* **2014**, *10*, 819–830.

(88) Dorenbos, G.; Suga, Y. Simulation of equivalent weight dependence of Nafion morphologies and predicted trends regarding water diffusion. *J. Membr. Sci.* **2009**, *330*, 5 – 20.

(89) Wu, D.; Paddison, S. J.; Elliott, J. A. Effect of Molecular Weight on Hydrated Morphologies of the Short-Side-Chain Perfluorosulfonic Acid Membrane. *Macromolecules* **2009**, *42*, 3358–3367.

(90) Wu, D.; Paddison, S. J.; Elliott, J. A.; Hamrock, S. J. Mesoscale Modeling of Hydrated Morphologies of 3M Perfluorosulfonic Acid-Based Fuel Cell Electrolytes. *Langmuir* **2010**, *26*, 14308–14315, PMID: 20704341.

(91) Kreuer, K.-D.; Paddison, S. J.; Spohr, E.; Schuster, M. Transport in Proton Conductors for Fuel-Cell Applications: Simulations, Elementary Reactions, and Phenomenology. *Chem. Rev.* **2004**, *104*, 4637–4678, PMID: 15669165.

(92) Paddison, S. Proton Conduction Mechanisms at Low Degrees of Hydration in Sulfonic AcidBased Polymer Electrolyte Membranes. *Annu. Rev. Mater. Res.* **2003**, *33*, 289–319.

(93) Maalouf, M.; Sun, C. N.; Pyle, B.; Emery, M.; Haugen, G. M.; Hamrock, S. J.; Zawodzinski, T. A. Factors enabling high mobility of protons and water in perfluorosulfonate membranes under low hydration conditions. *Int. J. Hydrogen Energy* **2014**, *39*, 2795–2800.

(94) Kreuer, K.-D.; Dippel, T.; Meyer, W.; Maier, J. Nafion Membranes: Molecular Diffusion, Proton Conductivity and Proton Conduction Mechanism. *MRS Proceedings* **2011**, *293*, 273–282.

(95) Madsen, L. A.; Hou, J. *Diffusion NMR of Confined Systems: Fluid Transport in Porous Solids and Heterogeneous Materials*; The Royal Society of Chemistry, 2017; pp 464–496.

(96) Li, J.; Park, J. K.; Moore, R. B.; Madsen, L. A. Linear coupling of alignment with transport in a polymer electrolyte membrane. *Nat. Mater.* **2011**, *10*, 507–511.

(97) Perrin, J.-C.; Lyonnard, S.; Guillermo, A.; Levitz, P. Water Dynamics in Ionomer Membranes by Field-Cycling NMR Relaxometry. *J. Phys. Chem. B* **2006**, *110*, 5439–5444, PMID: 16539481.

(98) Lee, D. K.; Saito, T.; Benesi, A. J.; Hickner, M. A.; Allcock, H. R. Characterization of Water in Proton-Conducting Membranes by Deuterium NMR T1 Relaxation. *J. Phys. Chem. B* **2011**, *115*, 776–783, PMID: 21218813.

(99) Trigg, E. B.; Tiegs, B. J.; Coates, G. W.; Winey, K. I. High Morphological Order in a Nearly Precise Acid-Containing Polymer and Ionomer. *ACS Macro Lett.* **2017**, *6*, 947–951.

(100) Trigg, E. B.; Gaines, T. W.; Maréchal, M.; Moed, D. E.; Rannou, P.; Wagener, K. B.; Stevens, M. J.; Winey, K. I. Self-assembled highly ordered acid layers in precisely sulfonated polyethylene produce efficient proton transport. *Nat. Mater.* **2018**, *17*, 725–731.

Graphical TOC Entry